LAMINAR BURNING VELOCITY AND MARKSTEIN LENGTH CHARACTERISATION OF STEELWORKS GAS BLENDS

D. Pugh,   A. P. Crayford,   P. J. Bowen,   T. O'Doherty,   R. Marsh,   J. Steer

Cardiff School of Engineering, Cardiff University, Wales, UK, CF24 3AA.
Corresponding author: D. Pugh. email: pughdg@cardiff.ac.uk;
Tel. +44(0) 2920 870 597

ABSTRACT

An outwardly propagating spherical flame configuration has been used to characterise the combustion of different blended steelworks gas compositions, under atmospheric ambient conditions. A nonlinear extrapolative technique was used to obtain values of laminar burning velocity and Markstein length for combustion with air and change in equivalence ratio. Peak burning velocity was shown to reach almost 1 m·s^{-1} for the combustion of coke oven gas under marginally rich conditions, and the influence of flame stretch on burning velocity also shown to increase with equivalence ratio. The molar fraction of coke oven gas was then blended in the range 0-15% with four blast furnace gas mixtures containing 1-7% H$_2$ fractions, representative of the inherent compositional fluctuation experienced in production. Profiles for change in burning velocity resulting from this addition of COG are presented, and the dampening extent of fluctuation resulting from the H$_2$ variation has been quantified. Results are also presented for the relative change in gross calorific value and corresponding Wobbe index of the variable blended gases across the tested limits. Modelled results were generated using the PREMIX coded CHEMKIN-PRO, and the performance of specified chemical reaction mechanisms evaluated relative to the experimental data.

Keywords:
Laminar burning velocity, Outwardly-propagating spherical flame, flame stretch, Blast furnace Gas, coke oven gas.

NOMENCLATURE

Abbreviations:
BFG   Blast Furnace Gas
COG   Coke Oven Gas

Symbols:

A	Spherical flame Area
CV_G	Gross Calorific Value
L_b	Markstein length
P	Initial pressure
T	Initial temperature
r_{sch}	Schlieren radius
S_u	Unstretched flame speed
S_n	Stretched flame speed
SG_{air}	Specific Gravity in relation to air
t	Time
WI_G	Gross Wobbe Index
α	Flame stretch-rate
u_l	Laminar burning velocity
ρ_b	Density of the burned gas
ρ_u	Density of the unburned gas
ϕ	Equivalence ratio

1. INTRODUCTION

The Steel industry is estimated to account for 6-7 % of global anthropogenic CO$_2$ emissions [1], with various techniques applicable for the process. The primary integrated works method of reducing ores in a blast furnace, followed by decarburisation, is the least efficient technique, and widely employed in almost 50 countries throughout the world. The approach recommended by the Intergovernmental Panel on Climate Change to improve efficiency is a combination of best available technologies, and maximising the use of by-products indigenous to the integrated works method [2]. Two of the chief by-products are fuels generated at different stages in the process, and are investigated in this study.

Blast Furnace Gas (BFG) results from the ferruginous reduction of iron ores with coke, and other resources. Preheated air (the blast) is introduced to the furnace

through base-level tuyeres, with upward gaseous flow catalysing reactions to form molten pig-iron, and simultaneously produce the by-product [3]. Volumetric BFG composition typically comprises a significant quantity of diluent CO_2 and N_2 (75%), with remaining fractions of CO, and a small variable percentage of H_2 (1-7%) [4, 5]. Consequently, the calorific value of BFG is low, however its significance results from the vast quantities continuously produced.

Coke Oven Gas (COG) is generated through destructive distillation of coal, as a result of the high temperature carbonisation process undertaken for the production of metallurgical coke. The resultant gaseous composition contains much larger fractions of combustible constituents, predominantly H_2, together with CO, CH_4 and other higher hydrocarbons [4].

Typically the gases will be used to fuel steelmaking process operations, however surplus gas can be used in power plants, with improvements in efficiency offering potential for significant energy savings. This increases the importance for investigation into the variable performance of steelworks gases as fuels. This is something that can potentially act to dissuade engineers from usage in more complex technologies, leading to more research in this area. [4-8].

1.1 Aim of this work

A fundamental physiochemical property of a fuel often used to characterise combustion performance is the Laminar burning velocity (u_L), and is directly related to operational instabilities such as blow-off and flashback [9, 29]. Previous work undertaken by the authors quantified the significant changes in u_L possible with small variation of H_2 fraction within BFG composition, inherent from operational changes made to the blast furnace [10]. Figure 1.1 presents the fluctuation in u_L for BFG comprising molar fractions of 23% CO and CO_2, 54% N_2, with displacing H_2 added in the range of 1-7%, for atmospheric conditions.

The results show a possible rise in u_L of over 200% as H_2 fraction increases across the tested limits. The aim of the current work is to quantify the effectiveness of blending
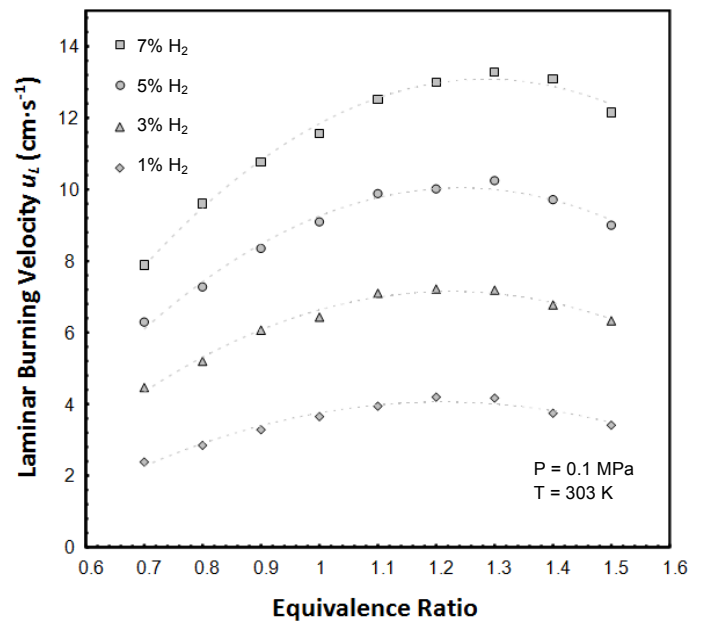

Figure 1.1 laminar burning velocities of different BFG compositions [9]

small amounts of COG to dampen out this fluctuation for the same level of compositional variation. This was achieved by applying the widely used method of analysing propagation of spherical flames within a constant-volume combustion bomb. This technique also allows for examination of the influence of stretch on flame speed, as quantified by the burned gas Markstein length (L_b) [11-26].

Results are presented for blends of COG and BFG in different ratios, at ambient conditions of 303 K and 0.1 MPa. The same four BFG H_2 fractions were tested, with COG added in the range of $0 - 15$ % of total fuel fraction. The molar fractions of all tested fuel compositions, including the specified COG values (from [5]), are shown in Table 1.1.

The fluctuation in additional fuel characteristics of gross calorific value and corresponding Wobbe index have also been calculated for all tested fuels. Comparisons were made with several published chemical reaction mechanisms using the PREMIX coded CHEMKIN-PRO package, aiming to assess the most suitable for modelling steelworks gas combustion.

Table 1.1 Certified molar compositions of Fuels tested in this study

BFG H₂ %		1				3				5				7			
COG %	100	0	5	10	15	0	5	10	15	0	5	10	15	0	5	10	15
CO_2	0.015	0.232	0.222	0.211	0.200	0.228	0.217	0.207	0.196	0.223	0.213	0.202	0.192	0.219	0.208	0.198	0.188
N_2	0.040	0.530	0.505	0.481	0.456	0.519	0.495	0.471	0.447	0.508	0.485	0.461	0.438	0.497	0.475	0.452	0.429
CO	0.071	0.228	0.220	0.212	0.204	0.223	0.216	0.208	0.200	0.219	0.211	0.204	0.196	0.214	0.207	0.200	0.193
CH_4	0.256	0.000	0.013	0.025	0.039	0.000	0.013	0.025	0.039	0.000	0.013	0.026	0.039	0.000	0.013	0.025	0.038
H_2	0.618	0.010	0.040	0.071	0.101	0.030	0.059	0.089	0.118	0.050	0.078	0.107	0.135	0.070	0.097	0.125	0.152

2. MATERIAL AND METHODS

A schematic layout of the constant-volume combustion bomb used in this study is shown with additional components in Figure 2.1. The cylindrical bomb has a working volume of approximately 34 L, an internal diameter of 260 mm, and is designed to allow for a sufficiently long experimental time window in the pressure unaffected region of flame expansion [27, 28]. Eight external band-heaters and four thermocouples are employed in a PID control system to regulate the ambient temperature of the internal reactants.
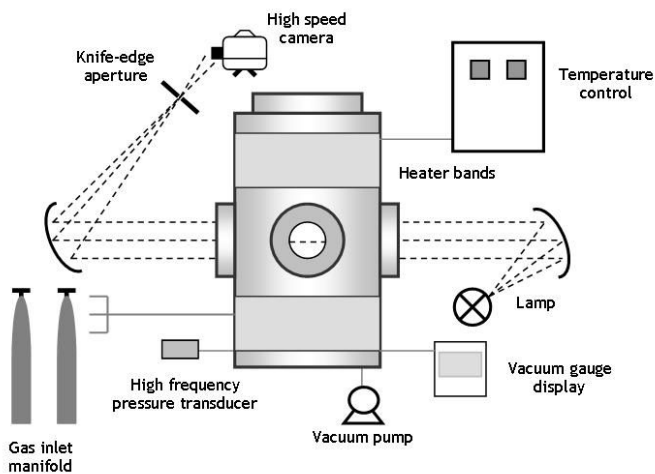
Figure 2.1 Diagrammatic layout of CVCB with ancillary components

Diametrically opposed windows allow for high-speed capture of flame propagation through the use of a widely employed Schlieren optical technique [11-20]. The method generates an image of the working area in a collimated light beam, exploiting the change in refractive index resulting from variation in gas density. A converging mirror is used to collimate a light source through 100 mm quartz viewing windows, with a secondary reflection then used to focus the light beam onto an aperture. The refracted portion of the beam unblocked by the edge focuses imperfectly, thereby creating light intensity gradients. These produce edges used to identify the isotherm representative of the flame front boundary [18]. The light is captured by a charge-coupled device in a Photron FASTCAM APX-RS high-speed camera. The system accommodates a spatial resolution of 0.14 mm per pixel, with diametric propagation rates obtained through bespoke software employing commercially available edge-detection algorithms.

Gas mixtures were introduced to the system through a manifold with a fine needle valve control. The constituent

fuel fraction and equivalence ratios were controlled by filling the chamber to calculated values of partial-pressure. This is enabled through the use of an ASG 0-2000 mbar sensor, with a resolution of 0.1mbar, and a real-time TIC 3 instrument controller readout. Between each test the CVCB was evacuated twice, firstly to remove the products from the previous test, then again subsequent to purging with compressed air to account for errors arising from imperfect vacuum (<1%). This meant the residual pressure remaining after the second evacuation could be added to the air fraction of the partial-pressure calculation, with a resultant contamination error in the order of 0.01 %. Adjacent internal fans are then used to blend the gases after filling to the required ratios.

Capacitor discharge ignition was achieved through the use of a variable voltage supply and fine electrodes introduced at 45° to the plane of measurement. Experiments were triggered by simultaneous 5 V signals from a pulse generator, feeding both ignition and data acquisition systems.

3. NUMERICAL THEORY

Results were obtained from the optical system in the form displayed in Figure 2.2. The shadowed edge of each frame is computationally scaled, eventually giving values for the propagating Schlieren radius (r_{sch}). Limits were set on the range of usable radii in order to account for the spark influence during early flame growth, and the confinement affects of pressure increase from the chamber walls. It has been shown [18] that the growth rate of flame kernels can be spark affected up to a radius of approximately 6 mm, and with a sensitivity factor included, 8 mm was chosen as the minimum radius for observation in this study. The maximum usable radius was specified, again with a safety factor, to be 35 mm. This follows from the calculated maximum equal to 39 mm as given by the recommended limit of 30% of the cylindrical chamber radius [27].
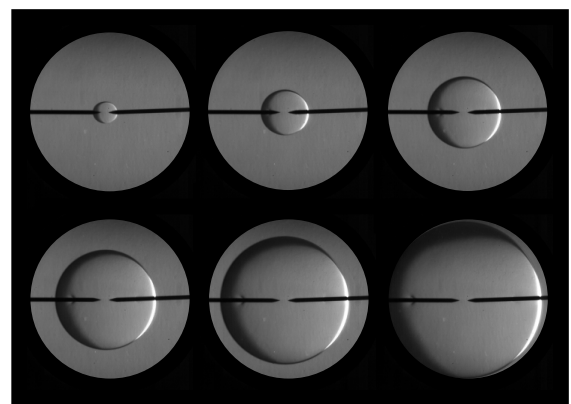
Figure 2.2 Examples of images obtained from the Schlieren optical system

For a centrally-ignited outwardly propagating spherical flame, the rate of expansion is influenced by the combined affects of curvature, instability, and flow-field strain [9]. The influence of this flame stretch on propagation rate has to be quantified and negated in order to obtain values for u_L. Firstly the stretched flame speed (S_n), can be attained from the temporal derivative of flame radius as follows:

$$S_n = \frac{dr_{sch}}{dt} \tag{1}$$

In this study the change in S_n was calculated as the regressed differential of a 3rd order polynomial fitted to the plotted radii against time. The flame stretch rate (α) is defined as the change in spherical area gradient of the flame [9], and defined in relation to S_n thus;

$$\alpha = \frac{1}{A}\frac{dA}{dt} = \frac{2}{r_{sch}}\frac{dr_{sch}}{dt} = \frac{2}{r_{sch}}S_n \tag{2}$$

The relationship between α and S_n are numerically processed to attain values for the unstretched flame speed (S_u). For the purposes of this study, a nonlinear association is applied, as proposed by Kelley and Law [24], following from the work of Ronney and Sivashinsky [25]:

$$\left(\frac{S_n}{S_u}\right)^2 ln\left(\frac{S_n}{S_u}\right)^2 = -\frac{2L_b\alpha}{S_u} \tag{3}$$

This results from the observable nonlinearity in the plotted data when flames are heavily influenced by stretch, and resembles other similar associations for normalised flame speed in alternative configurations, such as counter-flow burners [24]. Eqn. (3) tends toward the widely employed linear methodology [11-26] when the influence of stretch on flame speed is small [21,24]. A nonlinear regressive technique was used in to fit the relationship of S_n and α to obtain values for S_u and L_b, with the latter specified as the downstream, or burned Markstein length, and acts to quantify the influence of stretch on flame speed.

In order to attain values for laminar burning velocity (u_L) from derived S_u, fuel expansion must be negated to measure the velocity of the flame relative to the unburned fuel, and at constant pressure can be accounted for by the density ratio of burned (ρ_b) to unburned gas (ρ_u):

$$u_L = S_u\left(\frac{\rho_b}{\rho_u}\right) \tag{4}$$

Adiabatic gas densities were calculated theoretically (consistent with comparative works [11-26]) using a flame configuration utilised in the CHEMKI-PRO package. Different chemical reaction mechanisms were used by the software for this part of the study, and the employed model specifications and selection of each mechanism are discussed further in section 4. The performance of the described experimental system and methodology has been benchmarked against analogous literature, with results highlighted by Pugh *et al* [10].

The gross calorific value (CV_G) of each composition was calculated for ideal mass fractions, and normalised to IUPAC standard conditions of temperature and pressure (273 K, 0.1 MPa) [30]. This value was then used to calculate the gross Wobbe Index (WI_G) for that composition:

$$WI_G = \frac{CV_G}{\sqrt{SG_{air}}} \tag{5}$$

Where SG_{air}, corresponds to the specific gravity of the mixture in relation to the density of air (calculated as 1.276 kg·m^{-3}).

4. RESULTS AND DISCUSSION

Results are principally provided in numerical tables due to the large number of fuel compositions tested, with selected data plotted to demonstrate trends.

4.1 COG Results

Firstly, experiments were performed with the specified COG mixture to determine the order of difference in u_L between these values and BFG. Figures 4.1 and 4.2 show examples of plotted of S_n against α for the combustion of COG/air with increasing equivalence ratio ranging from 0.7 to 1.5, and the superimposed nonlinear relationship given in Eqn. (3). The data is separated into two plots for clarity.
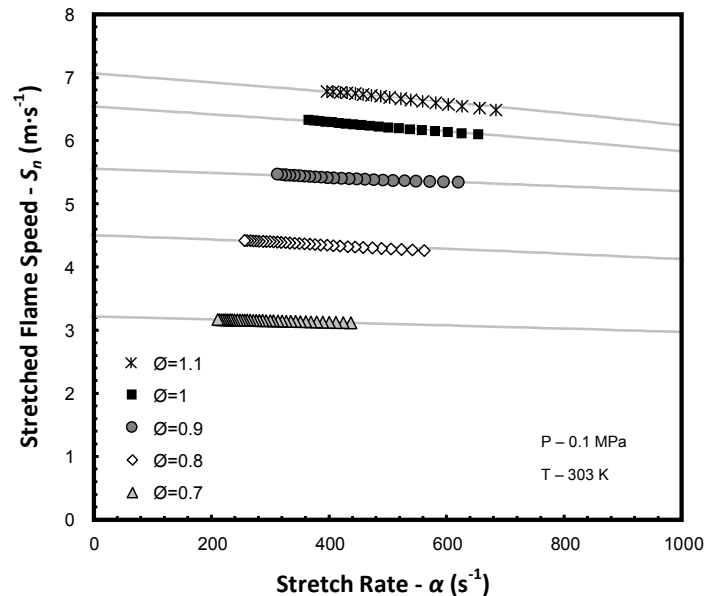

Figure 4.1 Examples of S_n plotted against α for COG combustion, $\varnothing = 0.7 - 1.1$
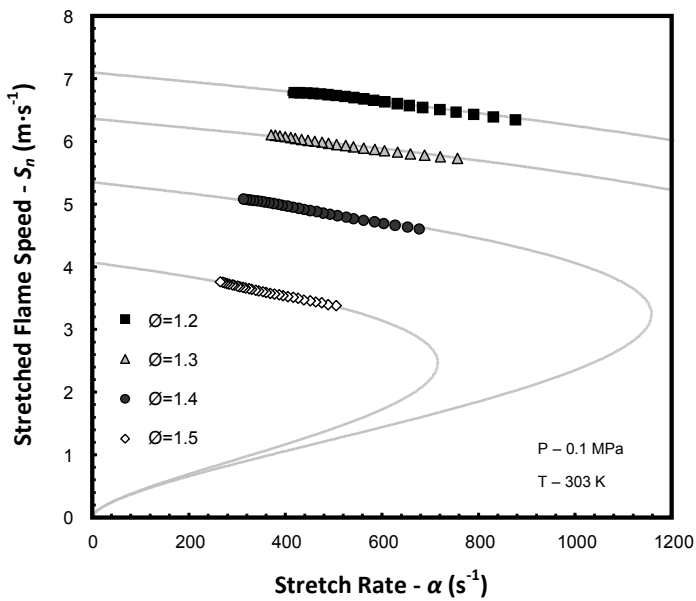
Figure 4.2 Examples of S_n plotted against α for COG combustion, $\emptyset = 1.2 - 1.5$

The data points in each figure are attained from individual frames in the high-speed video file, which for COG were captured at 7,000 fps. The gradient of each plot relates directly to L_b, inasmuch that as the incline increases, the effects of stretch are more influential on flame speed. It is evident from Figures 4.1 and 4.2 that this becomes more significant with richness for COG flames, and is fully quantified in Figure 4.3 where average experimental L_b is plotted against equivalence ratio.
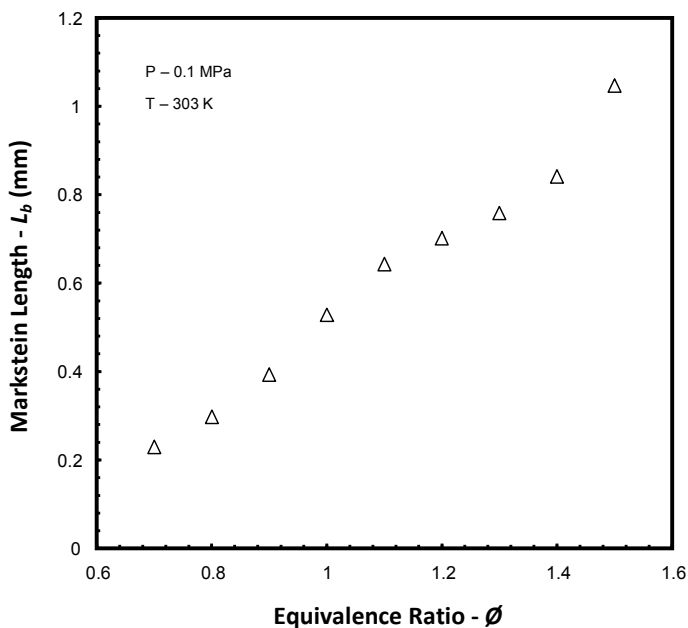

Figure 4.3 Average experimental COG L_b plotted against $\emptyset$

Change in L_b results from variation in the mixture's ratio of thermal to mass diffusivity, defined as the Lewis number (Le) [9]. When these properties are equal, the mixture can be defined as equidiffusive and the influence of flame stretch minimised, occurring under leaner conditions for the combustion of COG. The observations are interesting as the most significant fuel fraction is H_2, which is more than double the nearest constituent CH_4 fraction; and an increase in H_2 tends to provide a decrease in the measured L_b, as was seen with BFG results and data from other institutions [10-13]. However, the negative offset in L_b resulting from H_2 addition is increased by the presence of heavier inert diluents in the fuel [11-13], which is minimal for COG (respective molar CO_2 and N_2 fractions of 1.5 and 4 %), with heat release from combustible constituents increasing the relative influence of thermal diffusivity.

The adiabatic gas density ratio was attained through use of the GRI-Mech 3.0 [31] reaction mechanism, optimised to model the combustion of natural gas, and employing 53 chemical species in 325 reactions. Figure 4.4 gives the consequential values of u_L attained from S_u, together with modelled results.
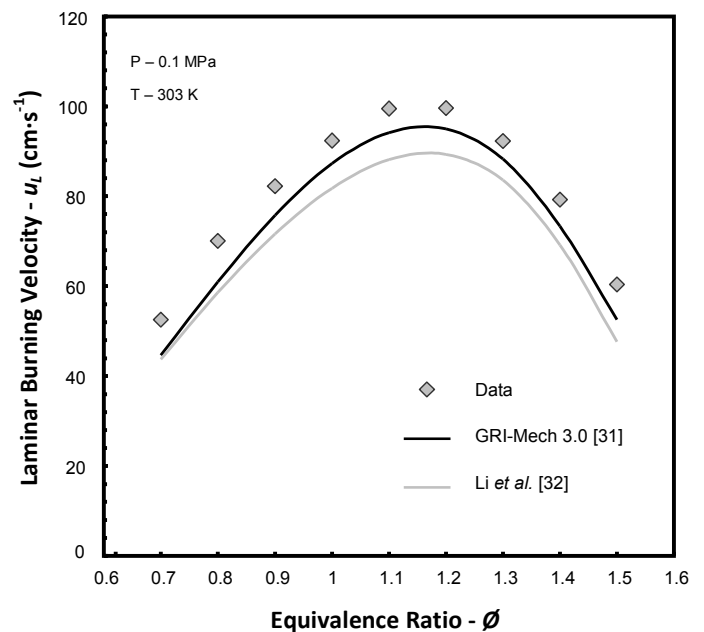

Figure 4.4 Average experimental COG u_L plotted against $\emptyset$

Figure 4.4 also shows the results obtained by the Li *et al.* [32] reaction mechanism with C1 species (21 in total, in 93 reactions), which compares poorly to the GRI-Mech model and experimental data. However, this mechanism is designed primarily for the combustion of CO, and consequently has been shown to perform well for modelling BFG [10]. The highest value of u_L is appears under marginally rich conditions at the hottest flame temperature

[29,9]. The curve also demonstrates significant variation across the tested range of equivalence ratios, with peak u_L effectively doubling from the value at $\emptyset$=0.7. Typically u_L peaks around $\emptyset$ = 1.75 for H_2 flames, however the observed characteristic behaviour is closer to combustion of CH_4. This suggests the other smaller molar fractions of the COG composition significantly influence the mixture diffusivity compared to the preponderant H_2 [9]. The numerical results obtained for S_u, applied density ratio, and u_L are provided in table 4.1.

Table 4.1 COG results

| $\emptyset$	S_u (cm·s^{-1})	$\left(\dfrac{\rho_b}{\rho_u}\right)$	u_L (cm·s^{-1})
0.7	316.15	0.166	52.60
0.8	452.64	0.155	70.06
0.9	562.32	0.146	82.27
1	654.79	0.141	92.37
1.1	708.78	0.140	99.48
1.2	699.07	0.142	99.59
1.3	635.58	0.145	92.27
1.4	535.09	0.148	79.22
1.5	399.84	0.151	60.39

4.2 BFG and COG Blends

The high-speed frame capture rate was decreased to 3,000 fps for the blended mixtures, with four equivalence ratios tested. These ratios were specified as lean, rich, stoichiometric, and approximate peak (0.8, 1.4, 1, and 1.2 respectively). Figure 4.5 gives examples of plotted S_n against α, for BFG containing 1 and 7 % H_2 at two different equivalence ratios, and the four different levels of COG addition.

These data are plotted as they provide a limited behavioural overview of the blended fuels. The BFG mixture containing 1 % H_2 exhibits a significant sensitivity to COG addition, with changes in both the influence of stretch and flame speed, where as the 7 % mixture exhibits a less significant change in gradient. This suggests adjustments to diffusivity and reaction chemistry are more significant when quantities of H_2 are initially low (for $\emptyset$ = 1, and 1.2). It was only under the richest conditions that COG addition began to display a more heavy change in values of L_b for the 7 % H_2 BFG mixture. Furthermore, the difference in gradient between each of the heavily COG diluted mixtures is also reduced, and this can be seen in the plotted example values in Figure. 4.6. There is a converging trend visible in the data as the influence of stretch becomes more uniform, and the variation between combustible fractions is reduced.
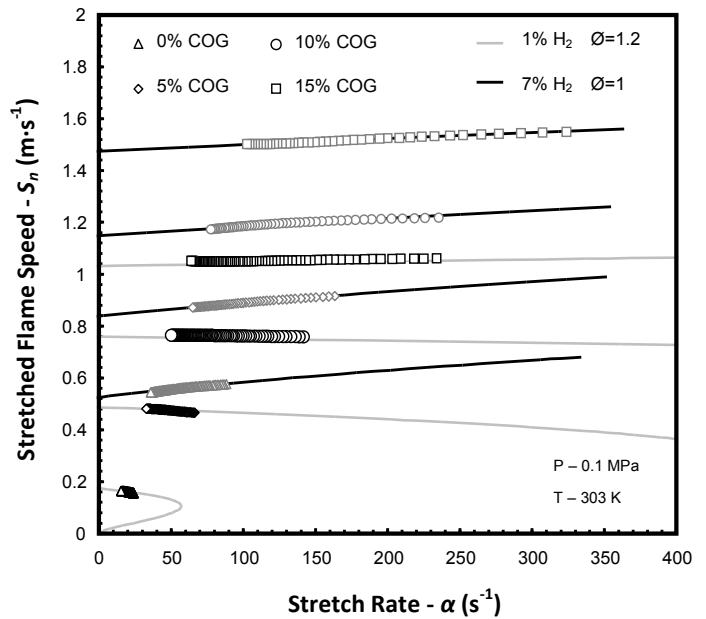
Figure 4.5 Examples of S_n plotted against α for combustion COG/BFG blends
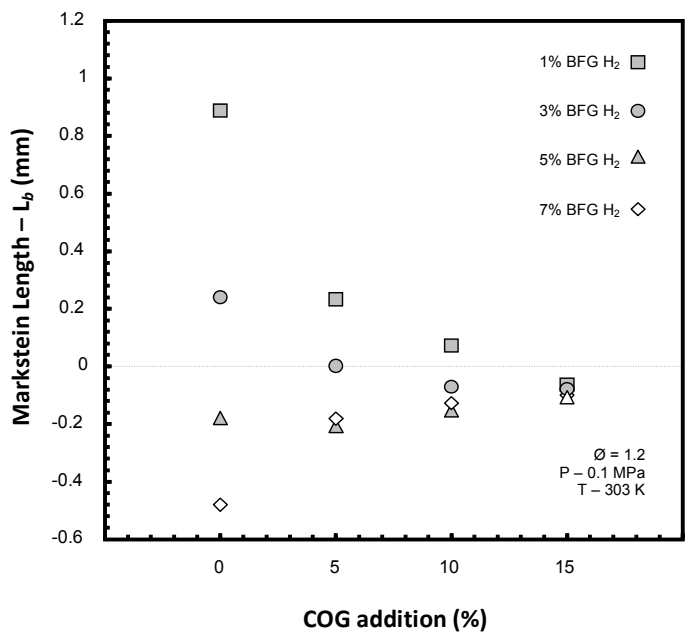
Figure 4.6 Examples of BFG L_b against COG addition for $\emptyset$ = 1.2

This convergence of L_b with increasing COG addition is expected as fuel blends begin to equalise; however the absolute change is disproportionate to the level of COG addition, with values also approaching a point much lower

6

than for the pure mixture (for the $\emptyset$ = 1.2 example in Figure 4.6, values approach -0.1, compared to ~0.7 for the corresponding 100% COG value). This emphasises the overriding effect of the preponderant H_2, causing stretched propagation to be more heavily influenced by mass diffusion when the mixture contains high concentrations of heavy inert species (as discussed in section 4.1) [10-13]. The same trend for convergence in values was seen for all equivalence ratios, with the focal point effectively rising with richness ($\emptyset$=0.8:≈-0.8, $\emptyset$=1:≈-0.4, $\emptyset$=1.2:≈-0.1 (as shown in Figure 4.6), $\emptyset$=1.4:≈0.7). This is advantageous, because as well as potentially dampening the amount of relative change in flame speed, COG addition also lowers fluctuation in the influence of flame stretch induced from change in BFG H_2 concentration.

COG addition appears to yield an almost linear increase in flame speed. This is shown with examples of stoichiometric data for S_u, and corresponding values of u_L in Figures 4.7 and 4.8 respectively. The density ratios applied to obtain these data were modelled using the Li *et al.* mechanism, because of its superior performance when modelling BFG [10]. However, any difference in obtained densities between reaction mechanisms is negligible compared to the resolution of the presented data (<0.1 %).
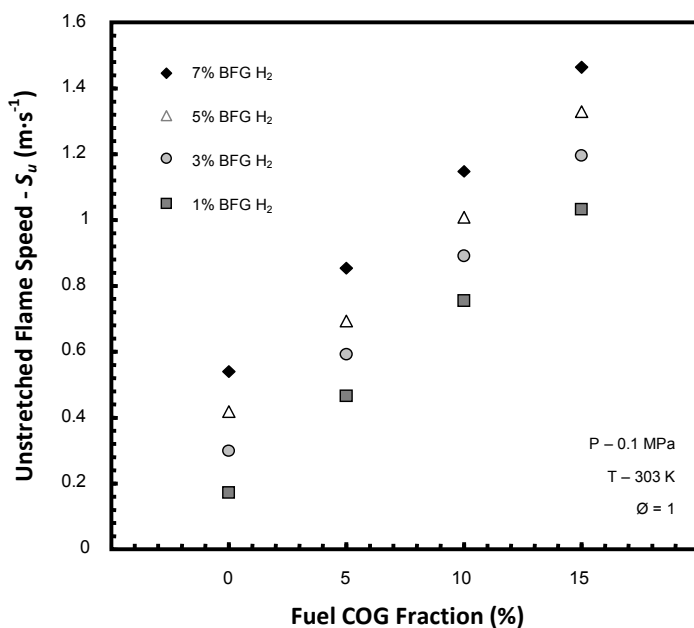

Figure 4.7 S_u plotted against COG fraction for combustion of stoichiometric COG/BFG blends
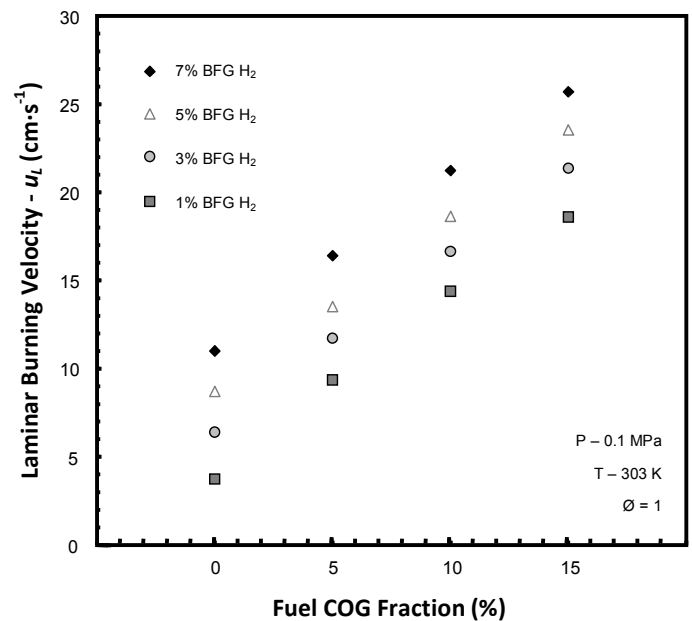

Figure 4.8 u_L plotted against COG fraction for combustion of stoichiometric COG/BFG blends

There are similar trends observed for all blends and equivalence ratios, with the near linear increase in flame speed for the addition of COG. Whilst the offset between each BFG mixture appears near parallel, there is some expected minor convergence as values tend towards those measured for baseline COG results presented in section 4.1. Nevertheless the increase in S_u with COG addition is significant, particularly for low H_2 BFG, as speeds rise by over a factor of five across the tested 0-15 % range. The mixtures comprising both high levels of BFG H_2, together with 15 % addition of COG are of an order approaching the equivalent values for combustion of methane/natural gas (~37 cm·s^{-1}) [10, 20].

Figure 4.9 gives an example of the changing profiles for plotted u_L against $\emptyset$ corresponding to the 1 % H_2 BFG mixture, and increasing quantities of COG. The rise in curvature of each plot suggests supplementing the COG fraction yields larger absolute variation in u_L with $\emptyset$. The peak of each curve also appears to shift marginally towards leaner ratios, as would be expected with data tending toward the plot in Figure 4.4.
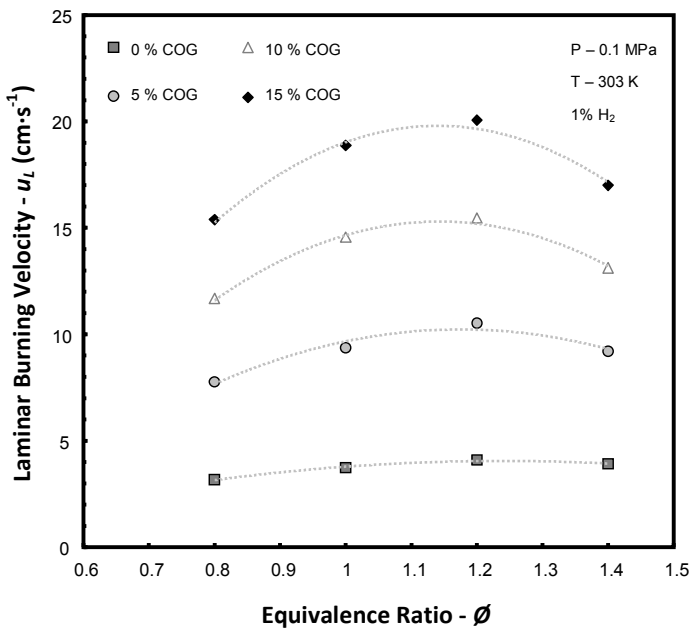
Figure 4.9 u_L plotted against $\varnothing$ for combustion of COG/BFG blends

The lines are superimposed to help separate each set, with similar trends also evident when plotting the alternative BFG compositions. The entire averaged database for all blends tested is provided in Table 4.2.

The relative performance of each chemical reaction mechanism in modelling COG and BFG blends, as to be expected, changes with composition. The Li *et al.* mechanism offers better correlation with no COG addition, and then is surpassed by the GRI-Mech model as the blended ratio increases. This trend is shown in Figure 4.10 where the 1 and 7 % H$_2$ fractions are plotted for $\varnothing = 1.2$.
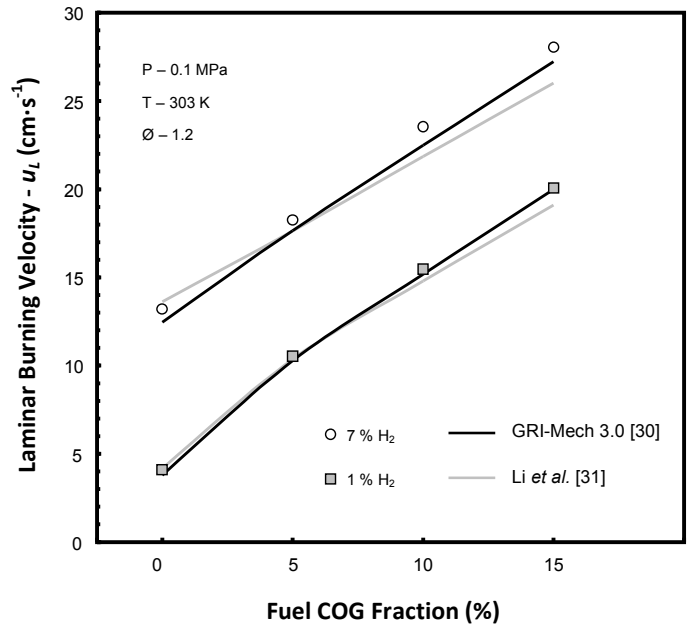
Figure 4.10 Performance of models for COG/BFG blends

Table 4.2 COG/BFG Blend results

$\varnothing$	BFG H$_2$ % / COG %	1				3				5				7			
		0	5	10	15	0	5	10	15	0	5	10	15	0	5	10	15
0.8	S_u (cm·s^{-1})	13.96	36.64	58.15	79.83	23.05	42.96	66.12	87.69	31.64	53.72	78.45	101.27	42.66	65.37	89.42	13.96
1		17.17	46.54	75.95	103.24	30.04	59.26	89.11	119.59	41.79	69.35	100.83	132.93	53.74	85.37	116.21	17.17
1.2		17.48	48.70	76.19	104.06	29.78	60.48	89.63	117.91	43.69	73.27	102.48	135.48	58.66	88.58	120.34	17.48
1.4		15.59	39.59	60.18	82.11	27.26	52.82	73.26	93.20	40.26	62.81	85.03	107.74	55.45	77.02	99.39	15.59
0.8	$\left(\dfrac{\rho_b}{\rho_u}\right)$	0.227	0.212	0.201	0.193	0.223	0.209	0.199	0.191	0.219	0.206	0.197	0.190	0.215	0.204	0.195	0.188
1		0.218	0.201	0.189	0.180	0.213	0.198	0.187	0.179	0.209	0.195	0.185	0.177	0.205	0.192	0.183	0.176
1.2		0.234	0.216	0.203	0.193	0.229	0.213	0.200	0.191	0.224	0.209	0.198	0.189	0.220	0.206	0.196	0.187
1.4		0.251	0.232	0.218	0.207	0.246	0.228	0.215	0.205	0.241	0.225	0.212	0.203	0.236	0.221	0.210	0.201
0.8	u_L (cm·s^{-1})	3.17	7.76	11.69	15.39	5.14	8.98	13.15	16.77	6.93	11.08	15.44	19.22	9.18	13.31	17.44	20.83
1		3.74	9.36	14.38	18.60	6.41	11.72	16.65	21.36	8.72	13.52	18.63	23.54	11.01	16.41	21.24	25.70
1.2		4.10	10.53	15.46	20.07	6.83	12.86	17.96	22.51	9.81	15.34	20.28	25.61	12.91	18.26	23.54	28.05
1.4		3.92	9.20	13.12	17.00	6.70	12.07	15.77	19.09	9.69	14.12	18.06	21.83	13.08	17.04	20.85	24.13

Simple relative analyses of the effectiveness of COG in dampening the consequences of H_2 fluctuation have been performed, by quantifying the percentage change for each composition across the tested H_2 limits. For example, with no COG added, stoichiometric combustion of BFG shows an elevation in u_L from 3.74 to 11.01 cm·s^{-1}, or an increase of 195 % as molar BFG H_2 fraction is increased from 1 to 7 %. Figure 4.11 shows how this value decreases with COG addition for all Ø.
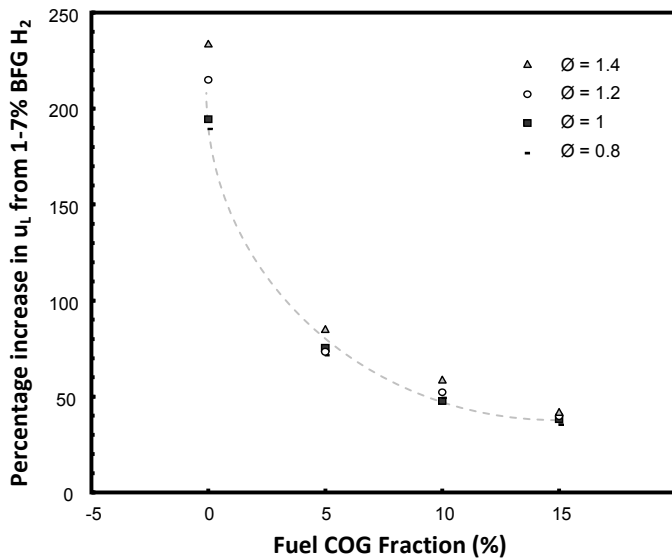

Figure 4.11 Percentage change in u_L for 1-7 % H_2

The relative change in u_L significantly decays as the COG fraction within the fuel rises. The percentage change in CV_G and corresponding WI_G have also been calculated in a similar way, and are shown in Figure 4.12, with the actual values provided in Table 4.3.
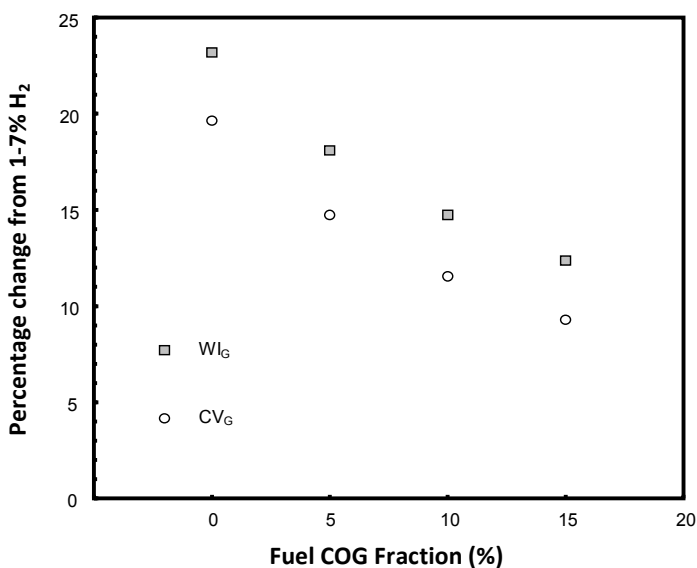

Figure 4.12 Percentage change in CV_G and WI_G for 1-7% H_2

Table 4.3 COG CV_G and WI_G

BFG %	COG %	0	5	10	15
1		2.96	3.75	4.54	5.32
3	CV_G (MJ· Nm^{-3})	3.16	3.93	4.71	5.49
5		3.35	4.12	4.88	5.65
7		3.54	4.30	5.06	5.82
1		2.84	3.66	4.52	5.40
3	WI_G (MJ· Nm^{-3})	3.06	3.88	4.73	5.62
5		3.28	4.10	4.95	5.84
7		3.50	4.33	5.18	6.07

The relative change in CV_G and WI_G decrease as COG fraction rises, and yields and overall increase in the energy density of the gas.

CONCLUSIONS

The constant volume bomb employed in this study used an outwardly propagating spherical flame configuration to characterise u_L and L_b profiles of a theoretical COG composition, first independently, and then blended with several representative BFG mixtures. This was to quantify the dampening influence in minimising fluctuation resulting from H_2 variation, inherent in the production of BFG. The study adds to data available in literature for the combustion of diluted syngases, and the following conclusions can be drawn:

- The study showed peak u_L values nearing 1 m·s^{-1} for COG combustion, observed under marginally rich conditions. These values are much higher than the equivalent for methane/natural gas increasing the propensity for premixed operational instabilities such as flashback. The influence of flame stretch on burning velocity was also shown to increase alongside mixture richness, with thermal conduction becoming more dominant in relation to mass diffusivity.

- The fractional increase of COG in the range 0-15 % was measured with four different BFG mixtures containing 1-7 % H_2. The obtained trends suggest the addition of small COG quantities can significantly dampen the relative fluctuation in burning velocity, experienced from changes in BFG H_2 fraction. COG addition also led to convergence of quantified L_b, diminishing the variable influence of flame stretch. Therefore, COG addition significantly stabilises the combustion of compositionally variable BFG.

- The 15 % addition of COG was also shown almost halve the fluctuation in Gross calorific Value and Wobbe index of the variable BFG mixture across the tested limit, whilst increasing the overall energy density. Results therefore suggest that blending mixtures of COG will also inherently stabilise any operational thermal output.

- The study finally allowed for analysis of how specified chemical kinetic mechanisms perform when modelling the combustion of complex gas mixtures. The GRI-MECH 3.0 mechanism offers better performance compared to the one published by Li *et al.* for modelling atmospheric combustion of COG. However, the Li mechanism is superior when modelling BFG, with values intersecting as blended COG levels are increased. This therefore suggests careful consideration must be given when selecting a mechanism to most accurately model these steelworks gas blends in any design process.

ACKNOWLEDGEMENTS

REFERENCES

[1] Kim, Y. Worrell, E. 2002 "International comparison of CO_2 emission trends in the iron and steel industry" Energy Policy: 30, 10, pp. 827-838.

[2] IPCC Fourth Assessment Report: Climate Change 2007. Intergovernmental Panel on Climate Change, Geneva, Switzerland.

[3] Biswas, A.K. 1981. "Principles of blast furnace Ironmaking: Theory and Practice" Cootha.

[4] IPPC, European Commission, "Best Available Techniques Reference Document on the Production of Iron and Steel" 2001.

[5] Ziebik, A. Stanek, W. 2003. "Identification of the influence of blast-furnace working parameters upon the supply and net calorific value of blast furnace gas". Acta Montanistica Slovaca, 4.

[6] Bonzani, F. Pollarolo, G. Rocca, F. 2002. "Operating Experience of Ansaldo V94.2 K Gas Turbine Fed by Steelworks Gas". ASME Conference Proceedings 2002(36061), pp. 203-208.

[7] Yongqi, L. Haifeg, W., and LI Ping, L..2007. "Study on Combustion Characteristics of the Blast Furnace Gas in the Constant Volume Combustion bomb" WSEAS International Conference on Power Systems, Beijing, China, 115.

[8] Liu, Y., Wang X., Zhu G, Liu R, Gao Z. 2011. "Simulation on the Combustion Property of Blast-Furnace Gas Engine by GT-POWER. Advanced Materials Research". Volumes 156 – 157, AMT . pp. 965-968.

[9] Law, C, K. "Combustion Physics", 2006. Cambridge University Press,

[10] Pugh, D. O'Doherty, T. Griffiths A. Bowen P. Crayford A. Marsh R. 2012. "Laminar burning velocity and Markstein length characterisation of compositionally dynamic blast furnace gas" proceedings of ASME Turbo Expo, GT2012-69667.

[11] Tahtouh,. F. Halter. E. Samson,. C. Mounaı¨m-Rousselle 2009 "Effects of hydrogen addition and nitrogen dilution on the laminar flame characteristics of premixed methane–air flames", International Journal of Hydrogen energy; 34: pp 8329-8388.

[12] Bouvet A., Chauveau C., Gokalp I., Halter F. 2011. "Experimental studies of the fundamental flame speeds of syngas (H2/CO)/air mixtures" Proceedings of the Combustion Institute; 33: pp.913–920.

[13] Qiao L, Kim C.H., Faeth G.M. 2005 "Suppression effects of diluents on laminar premixed hydrogen/oxygen/nitrogen flames" Combustion and Flame 143: pp.79–96.

[14] Ilbas M, Crayford AP, Yilmaz I, Bowen PJ, Syred N. 2006 "Laminar burning velocities of hydrogen–air and hydrogen–methane– air mixtures: an experimental study". International Journal of Hydrogen Energy; 31: pp.1768–79.

[15] Dowdy D.R., Smith D.B., Taylor S.C., Williams A.. 1991. "The use of expanding spherical flames to determine burning velocities and stretch effects in hydrogen/air mixtures", Symp (Int.) Combust. 23: pp.325–332.

[16] Brown M.J., McLean I.C., Smith D.B., Taylor S.C., 1996 "Markstein lengths of CO/H2/air flames, using expanding spherical flames", Symp. (Int.) Combust. 26: pp.875–881.

[17] Lamoureux, N., N. Djebaïli-Chaumeix, and C.E. Paillard,. 2003. "Laminar flame velocity determination for H2-air-He-CO2 mixtures using the spherical bomb method". Experimental Thermal and Fluid Science, 27(4): pp. 385-393.

[18] Bradley, D., Gaskell, PH, Gu, X,J. 1996. "Burning Velocities, Markstein Lengths, and Flame Quenching for Spherical Methane-Air Flames: A Computational Study" Combustion and Flame, 104, (1-2): pp 176-198.

[19] Bradley, D., Hicks, R., Lawes, M., Sheppard, C.G., Wooley, R. 1998 "The measurement of laminar burning velocities and Markstein numbers for iso-octane-air and iso-octane-n-heptane-air mixtures at elevated temperatures and pressures in an explosion bomb". Combustion and Flame,. 115(1-2): pp. 126-144.

[20] Gu, X., Haq, M., Lawes, M., Wooley, R. 2000. "Laminar burning velocity and Markstein lengths of methane-air mixtures" Combustion and Flame, 2000. 121(1-2): pp. 41-58.

[21] Halter, F., Tahtouh, T., and Mounaïm-Rousselle, C., 2010 "Nonlinear effects of stretch on the flame front propagation. Combustion and Flame". 157(10): pp. 1825-1832.

[22] Markstein GH. 1951. "Experimental and theoretical studies of flame-front stability". Journal of Aeronautical Science"; 18:pp.199–209.

[23] Tahtouh, T., Halter F., and Mounaïm-Rousselle C., 2009 "Measurement of laminar burning speeds and Markstein lengths using a novel methodology". Combustion and Flame, 156(9): p. 1735-1743.

[24] Kelley, A.P. and C.K. Law. 2009. "Nonlinear effects in the extraction of laminar flame speeds from expanding spherical flames". Combustion and Flame. 156(9): pp. 1844-1851.

[25] P.D. Ronney, G.I. Sivashinsky,. 1989. SIAM J. Applied Mathematics. 49 1029–1046.

[26] Prathap, C., A. Ray, and M.R. Ravi, Investigation of nitrogen dilution effects on the laminar burning velocity and flame stability

of syngas fuel at atmospheric condition. Combustion and Flame, 2008. 155(1-2): p. 145-160.

[27] Burke, M., Chen, Z., Ju. Y., Dryer, F., 2009. "Effect of cylindrical confinement on the determination of laminar flame speeds using outwardly propagating flames". Combustion and Flame, 156(4): pp. 771-779.

[28] Pink, I.P. 2006. Critical analysis of combustion characteristics of the Cardiff Cloud Combustor M.Phil. thesis. Cardiff University.

[29] Lieuwen, T. " Unsteady Combustor Physics", 2012, Cambridge University Press.

[30] International Union of Pure and Applied Chemistry Compendium of Chemical Terminology: Gold Book" 2012 version: 2.3.2.

[31] Bowman CT, Frenklach M, Gardiner WC, Smith GP.1999 The "GRIMech 3.0" chemical kinetic mechanism"; www.me.berkeley.edu/grimech.

[32] Li J., Zhao Z., Kazakov A., Chaos M., Dryer F.L., 2007 "A comprehensive kinetic mechanism for CO, CH2O, and CH3OH combustion". Int. J. Chem. Kinet. 39: pp.109–136.